의학박사 학위논문

MRI for Diagnosis and Treatment of Breast Cancer Stem Cells Using Multifunctional Nanoparticles

다기능성 나노입자를 이용한 유방암줄기세포의 자기공명영상 진단과 치료에 관한 연구

2015년 2월

서울대학교 대학원

의학과 영상의학

YUJIN SUN

다기능성 나노입자를 이용한 유방암줄기세포의 자기공명영상 진단과 치료에 관한 연구

지도교수 최 병 인

이 논문을 의학박사 학위논문으로 제출함

2014년 10월

서울대학교 대학원

의학과 영상의학

YUJIN SUN

YUJIN SUN 의 박사학위논문을 인준함

2014년 12월

위 원 장 (김 현진)

부위원장 (최병인)

위 원 (문 수정)

위 원 (문형순)

위 원 (허 용민)

MRI for Diagnosis and Treatment of Breast Cancer Stem Cells Using Multifunctional Nanoparticles

by

YUJIN SUN, M.D.

A Thesis Submitted to the Department of Medicine in Partial Fulfillment of the Requirements for the Degree of Doctor of Philosophy in Medical Science (Radiology) at Seoul National University College of Medicine

December 2014

Approved by Thesis Committee:

Professor Hyeonjin Kim Chairman

Professor Byung Ihn CHOI Vice chairman

Professor

Professor

Professor Yong Min Huh

ABSTRACT

MRI for Diagnosis and Treatment of Breast Cancer Stem Cells Using Multifunctional Nanoparticles

YUJIN SUN, M.D.

Department of Medicine
The Graduate School
Seoul National University

Introduction: The identification of breast tumor initiating cells (BTICs) is important for diagnosis and therapy of breast cancers. This study was undertaken to evaluate whether the extra domain-B of fibronectin (EDB-FN) could be used as a new biomarker for BTICs and whether EDB-FN peptide conjugated superparamagnetic iron oxide nanoparticles (SPIONs) loaded with doxorubicin (Dox) could be used as a multifunctional magnetic resonance imaging (MRI) contrast agent for achieving simultaneous diagnostic imaging and therapeutic application of BTICs expressing EDB-FN *in vitro* and *in*

vivo .

Methods: The human breast cancer cell lines (MCF-7, BT-474, SUM-225, MDA-MB-231) and NDY-1 cells, which display the tumor-initiating abilities and drug resistance, isolated from the cancer tissues of a breast cancer patient were used. mRNA expressions were assessed by RT-PCR. ALDEFLUOR assay to measure ALDH1 activity was performed. A high-affinity and high-specificity peptide ligand for EDB-FN, designated as APT_{EDB} was synthesized. APT_{EDB} or $APT_{scramble}$-conjugated TCL-SPION (APT_{EDB}-TCL-SPION or $APT_{scramble}$-TCL-SPION) were developed for selective EDB-FN-targeted MRI. NDY-1 cells were subcutaneously injected into the back right flank of female BALB/c nude mice (4-5 week old) for xenograft tumor model. *In vitro* and *in vivo* MRI studies were performed by using a 3T clinical MR scanner. For the analysis of selective EDB-FN targeting MRI of BTIC tumors, T_2*-weighted images of tumor were obtained and the signal intensity changes of tumors were quantitatively analyzed before and after the intravenous injection with APT_{EDB}-TCL-SPION or $APT_{scramble}$-TCL-SPION. To examine the therapeutic efficacy of Dox-loaded TCL-SPIONs (Dox@APT_{EDB}-TCL-SPION or Dox@$APT_{scramble}$-TCL-SPION), *in vitro* cellular toxicity was assessed by a MTT assay and tumor volumes were measured after

three times administration of Dox@APT_{EDB}-TCL-SPION or Dox@$APT_{scramble}$-TCL-SPION into tail vein. After MRI examination, the histological analysis of the several tissues and tumors isolated from mice was performed.

Result: While BTICs (NDY-1) had abundant EDB-FN expressions, non-BTICs (MCF-7, BT-474, SUM-225, MDA-MB-231) did not. Transfection of the BTICs with EDB-FN siRNA significantly reduced the expression of EDB-FN and several genes related to BTIC markers, self-renewal, epithelial-mesenchymal transition and drug resistance. Furthermore, Cy3.3-labeled EDB-FN specific peptide (APT_{EDB}) showed preferential binding to the target NDY-1 cells. To construct an EDB-FN targeting imaging probe, APT_{EDB} was covalently attached to thermally cross-linked SPION (TCL-SPION) to yield APT_{EDB}-TCL-SPION. In the *in vitro* MRI of cell phantoms, selective binding of APT_{EDB}-TCL-SPION on NDY-1 cells was evident, but little binding was observed in MCF-7 cells. After the intravenous injection of APT_{EDB}-TCL-SPION to the xenograft NDY-1 tumor model in mice, significant signal decrease within the tumor was observed in T_2*-weighted images, but there was only a marginal signal change in the case of non-targeting SPIONs such as $APT_{scramble}$-TCL-SPION or TCL-SPION. In addition cell survival and tumor growth was remarkably inhibited in

the Dox@APT_{EDB}-TCL-SPION-treated group compare with untreated group and Dox@$APT_{scramble}$-TCL-SPION-treated group.

Conclusions: we report, for the first time, that EDB-FN is highly expressed in BTICs but not in differentiated breast cancer cells, suggesting that EDB-FN can be used as a new characteristic biomarker for identifying BTICs. Furthermore, we developed an imaging probe for targeting BTICs, which was constructed by covalently attaching EDB-FN specific high-affinity peptide to TCL-SPION and enabled visualization of BTICs within the tumor mass *in vivo* by a clinical 3T MR scanner. Furthermore, Dox@APT_{EDB}-TCL-SPION showed selective drug-delivery efficacy in the xenograft mouse model. The active tumor-targeting ability of Dox@APT_{EDB}-TCL-SPION allows for the selective detection of EDB-FN positive BTIC tumors by MRI as well as the effective delivery of anti-cancer drugs to the target tumor sites simultaneously. In the near future, we will study the therapeutic feasibility of APT_{EDB}-TCL-SPION combined with therapeutic drugs and EDB-FN RNAi as a novel theranostic system that allows for simultaneous diagnosis and therapy of hard-to-treat BTICs in breast cancers. The nanoparticle complexes loaded with specific ligand and therapeutic drugs and genes appears to have significant potential for the characterization of tumors and for the prediction of

prognosis in the context of treatment stratification and early assessment of tumor response to therapy.

Key words: Aptides, Breast tumor initiating cells, Extra domain-B of fibronectin, Superparamagnetic iron oxide nanoparticles, Magnetic resonance imaging, Doxorubicin

Student Number: 2013-30810

LIST OF TABLES AND FIGURES

LIST OF ABBREVIATIONS

MRI: magnetic resonance imaging

BTIC: Breast tumor initiating cell

TCL-SPION: thermally cross-linked-superparamagnetic iron oxide nanoparticle

FN: fibronectin

EDB: extra domain-B

EDA: extra domain-A

ALDH1: aldehyde dehydrogenase 1

PET: positron electron tomography

SPECT: single-photon emission computed tomography

RT-PCR: Reverse transcription polymerase chain reaction

CONTENTS

INTRODUCTION

Breast tumor initiating cells (BTICs), which can self-renewal and asymmetrically divide into differentiated cancer cells, are believed to be responsible for breast cancer progression, recurrence and therapeutic resistance [1-3]. BTICs with the CD44+ and CD24- signature, as well as high aldehyde dehydrogenase 1 (ALDH1) activity, are linked to many signaling pathways that regulate *in vivo* tumorigenicity, including invasiveness and metastasis, and are considered the major obstacle for curative treatments [1, 4]. However, the known biomarkers are insufficient for identifying BTICs, and additional, characteristic biomarkers are needed to develop new strategies for treating breast cancer and preventing recurrence.

Fibronectin (FN), a ubiquitous component of the extracellular matrix, plays major roles in cell adhesion, migration, and proliferation and also seems to play an important role in tumor progression [5]. Molecular variants of FN are generated by alternative splicing of pre-messenger RNA at three distinct sites, extra domain-A (EDA), extra domain-B (EDB) and type III homology connecting segment (IIICS) [6]. EDB-FN is not found in normal adult tissue, but it is highly expressed in the blood vessels

and extracellular matrixes of aggressive solid tumors, which makes the protein a promising tumor-associated biomarker [7-10]. In human breast tissues, EDB-FN is only found in fetal breasts, during the wound healing process, and in carcinomas [11, 12]. Based on known findings, we hypothesized that EDB-FN expression might also be associated with BTICs.

Superparamagnetic iron oxide nanoparticles (SPIONs) have been intensively used as magnetic resonance imaging (MRI) contrast agents for cancer imaging [13]. Furthermore, SPIONs, with the aid of specific ligands on their surface, can be used to detect the expression levels of specific biomarkers in tumors or on cancer cells [14]. We previously reported that thermally cross-linked SPION (TCL-SPION) are suitable MRI contrast agents for cancer imaging because they have higher transverse relaxivity and better biocompatibility than a commercially available SPION, MION-47 [15, 16]. We also demonstrated that TCL-SPION could be used as multifunctional nanoparticles, enabling simultaneous cancer imaging and therapy by loading therapeutic drugs and conjugating specific targeting moieties such as peptides and aptamers [17-19]. We also reported on a technology that enables the screening and identification of a novel class of high-affinity peptides ('aptides') for various biological targets [20]. Using platform technology, we

identified a high-affinity and high-specificity peptide ligand for EDB-FN, designated as APT_{EDB}, which is 26 amino acids long and has several tens of nM affinity for the protein [21, 22].

In this study, we evaluated whether EDB-FN could be used as a new biomarker for BTICs and whether EDB-FN peptide and Dox-loaded TCL-SPION could be used as a multifunction MRI contrast agents for BTIC -targeted imaging and therapy *in vitro* and *in vivo*. To this end, APT_{EDB}-TCL-SPIONs conjugated with an EDB-FN specific peptide ligand (APT_{EDB}) and Dox@APT_{EDB}-TCL-SPIONs loaded with Dox were prepared. This study revealed that APT_{EDB}-TCL-SPION could detect EDB-FN overexpressing BTICs (NDY-1 cells) *in vitro* and *in vivo* using MRI and Dox@APT_{EDB}-TCL-SPION displayed the a great therapeutic efficacy of BTICs *in vitro* and *in vivo* by a selective targeting of EDB-FN and an efficient delivery of anticancer drugs.

MATERIALS AND METHODS

Cell culture and reagents

MCF-7, BT-474, MDA-MB-231 cells were obtained from the Korean Cell Line Bank (Seoul, South Korea), and SUM-225 cells were purchased from Asterand, Inc. (Detroit, MI, USA). SUM-225 is a luminal subtype non-invasive cancer cell line, MCF-7 is a luminal subtype estrogen-dependent invasive cancer cell line, BT-474 is a luminal subtype invasive cancer cell line with ERBB amplification and MDA-MB-231 is a basal subtype invasive cancer cell line with metastatic potential [23]. These breast cancer cell lines were cultured in Dulbecco's modified Eagle medium (WelGENE, Daegu, South Korea) and supplemented with 10% fetal bovine serum (WelGENE) and a 1% antibiotic solution containing penicillin and streptomycin. NDY-1 cells which display the tumor-initiating abilities and drug resistance isolated from the breast cancer tissues of a human patient were kindly supplied by Dr. Noh of Seoul National University [24, 25] and were grown under nonadherent mammosphere culture conditions in serum-free Dulbecco's modified Eagle's medium (DMEM): F12 = 3:1 medium supplemented with B27 supplement (Invitrogen, Carlsbad, CA, USA), antibiotic-antimycotic (Invitrogen), 20 ng/ml epidermal growth factor (EGF; Invitrogen), 10 ng/ml leukemia inhibitory

factor (LIF, Millipore, Temecula, CA, USA), and 20 ng/ml basic fibroblast growth factor (bFGF; Millipore). The medium was replenished every 3-4 days. All cells were passaged weekly and cultured in a 5% CO_2 incubator at 37° C.

RT-PCR analysis

Total RNA was isolated from cells using the RNeasy Mini Kit (QIAGEN, Valencia, CA, USA). cDNA was synthesized using M-MLV reverse transcriptase (New England Biolabs, Ipswich, MA, USA) and random primers. The EDB-FN mRNA levels in breast cancer cells (SUM-225, MCF-7, BT-474, MDA-MB-231 and NDY-1) were evaluated using conventional RT-PCR. The specific primers for CD44, CD24, ALDH1A1, ALDH1A2, ALDH1A3, Nanog, Oct4, KLF4, c-Myc, N-cadherin, Twist, Slug, ABCG2, EDB-FN and β-actin are indicated in Table 1. Each target gene was amplified on a thermocycler (BioRad, Hercules, CA, USA). PCR products were analyzed using electrophoresis on 2% ethidium bromide-stained agarose gels, and the gene levels were normalized using β-actin.

ALDEFLUOR assay to measure ALDH1 activity

The ALDEFLUOR reagent system supplied by Stem Cell Technologies (Vancouver, Canada) was used in all experiments and offered an immunofluorescent method for detecting the intracellular enzyme activity of ALDH1. BODIPY-aminoacetaldehyde diethyl acetal (BAAA-DA) is converted to BODIPY-aminoacetaldehyde (BAAA), which is a fluorescent substrate for ALDH1, by treatment with 2 M HCl. In this study, we treated the cells as follows: 0.2-1.0 $\times$ 10^6 cells were kept in 1 ml of ALDEFLUOR assay buffer with a BAAA concentration of 1.5 μM for 45 minutes at 37° C. In each experiment, a sample of cells was stained under identical conditions with 50 μmol/l of the specific ALDH1 enzyme inhibitor, diethylaminobenzaldehyde (DEAB; Sigma, St. Louis, MO, USA), which served as a negative control. Flow cytometric analysis was performed.

Flow cytometry analysis

Flow cytometry was performed using a FACScan instrument (BD Biosciences, San Jose, CA, USA). NDY-1 cells were dissociated, washed once in phosphate buffered saline (PBS) containing 1-2% BSA and 5 mM EDTA and then stained with anti-CD24-FITC (Invitrogen) and anti-CD44-PE (Invitrogen) using 10 μl of antibody per 10^6 cells before they were incubated at 4° C for 15-30 minutes. Cells were washed once with PBS buffer, and flow

cytometry for $CD44^{+}CD24^{-}$ cells was performed using each fluorescence channel. Gates were determined by analyzing the unstained cells and single stains. ALDEFLUOR fluorescence was detected using the green fluorescence channel (530 ± 15). Data for 10,000 cells were collected and analyzed using Cell Quest software, version 3.3 (BD Biosciences).

siRNAs and transfection

The siRNA duplexes 5'-AAGGTATCCCTATTTTTGAAGCCTGTCTC-3' (sense) and 5'-AACTTCAAAAATAGGGATACCCCTGTCTC-3' (antisense) designed to knock down EDB-FN expression were synthesized by Bioneer (Seoul, Korea). Cells were transfected with siRNA and Lipofectamine-2000 according to the manufacturer's instructions. Briefly, cells were seeded in a 6-well-plate at a density of 2×10^5 cells/well with antibiotic-free medium 12 h before transfection. Mixtures of 20 μM siRNA, 1 μl of Lipofectamine-2000 and 50 μl of Opti-MEM medium (Invitrogen) were incubated at room temperature for 25 min to allow complex formation. After washing cells with PBS, 50 μl of each transfection mixture was added to each well, along with 950 μl of Opti-MEM medium, making the final concentration of 100 nM siRNA. The medium was replaced 24 h later by 1 ml of fresh culture medium. Cells were collected for

extraction of RNA and protein 48 h after transfection.

In vitro EDB-FN target imaging and immunocytochemistry

To test EDB-FN targeting ability of the APT_{EDB} (AnyGen, Gwangju, South Korea), cells were grown in 8-well chamber slides and treated with Cy3.3-labeled APT_{EDB} (6 μg/ml) in Opti-MEM (Invitrogen) for 6 h. After incubation, the cells were rinsed in PBS three times and fixed with 2% (w/v) paraformaldehyde. For the detection of EDB-FN protein, the fixed cells were incubated with primary antibodies directed against EDB-FN in cells, and staining was visualized with Alex 488-conjugated secondary antibodies (Invitrogen). 4' 6-diamidino-2-phenylindole (DAPI, Invitrogen) was used to visualize the cell nuclei. The fluorescence images were scanned and analyzed with a confocal laser microscope (LSM 5 META, Carl Zeiss, Jena, Germany).

Synthesis and characterization of EDB-FN aptide-conjugated TCL-SPION

TCL-SPION, APT_{EDB}-TCL-SPION and $APT_{scramble}$-TCL-SPION are kindly provided by Dr. Sangyong Jon of Korea Advanced Institute of Science and Technology. The typical synthesis procedure for EDB-FN aptide-conjugated TCL-

SPION was as follows: Carboxyl-TCL-SPION was synthesized as previously reported [15]. 1-ethyl-3-(3-dimethylaminopropyl) carbodiimide hydrochloride (15 mg) and sulfo-NHS (4 mg) were suspended in 200 μl of PBS and added to 1 ml of carboxyl-TCL-SPION in PBS (8 mg Fe/ml in PBS) and mixed by vigorously vortexing the sample. After 15 min, maleimide-PEG_{1000}-amine (4 mg in 100 μl dimethylformamide) was added to the solution and stirred at ambient temperature for 4 h. After the reaction was complete, the Mal-PEG_{1000}-TCL-SPION solution was passed through a 50 kDa centrifugal filter (Millipore) and dialyzed against distilled water (MW cut-off 100 kDa, Millipore) for 36 h to remove the unconjugated Mal-PEG_{1000}-amine from the carboxyl-TCL-SPION. Then, cysteinylated APT_{EDB} or $APT_{scramble}$ (0.1 mg) dissolved in dimethyl sulfoxide (100 μl) was added to Mal-PEG_{1000}-TCL-SPION (20 mg Fe/ml) dispersed in distilled water (0.5 ml). The solution was stirred for 4 h under ambient conditions; the reaction mixture was subsequently concentrated by filtration using a centrifugal filter (MW cut-off 50 kDa, Millipore) and washed with distilled water to yield APT_{EDB} or $APT_{scramble}$-conjugated TCL-SPION (APT_{EDB}-TCL-SPION or $APT_{scramble}$-TCL-SPION). The iron concentrations of APT_{EDB}-TCL-SPION or $APT_{scramble}$-TCL-SPION were measured using inductively coupled plasma-atomic emission spectrometry (ICP-AES, Perkin-Elmer,

Waltham, MA, USA). The hydrodynamic particle size and zeta potential of each SPION were measured using a Zetasizer ZS90 instrument (Malvern Instruments Ltd, Malvern, Worcestershire, UK). The magnetite core size and nanoparticle distribution were examined by transmission electron microscopy (TEM) using a Tecnai G2 F30 instrument operated at 300 kV (FEI company, Hillsboro, OR, USA).

To quantify the amount of aptide conjugated to the TCL-SPION, the amount of unreacted aptide remaining in the filtrate after the reaction between cysteinylated APT_{EDB} and Mal-TCL-SPION was measured using a UV-Vis spectrometer (SCINCO, Seoul, Korea). In this way, the amount of conjugated aptide was indirectly calculated using the following equation: $[APT_{EDB}]_{conjugated} = [APT_{EDB}]_{initial} - [APT_{EDB}]_{remained}$. The same procedure was performed using a mixture of cysteinylated APT_{EDB} and TCL-SPION lacking the maleimide functional group (no conjugation occurs). Then, the amount of APT_{EDB} in the filtrate was measured to assess the level of nonspecific physical binding of the aptide to the TCL-SPIONs, which was approximately 20%. Finally, the actual amount of the conjugated aptide on TCL-SPION was revised by considering the extent of the nonspecific binding.

Cell survival studies by MTT assay

In vitro cell survival was assessed using the 3-(4,5-dimethylthiazol -2-yl)-2,5-diphenyl tetrazolium bromide (MTT) assay . Briefly, NDY-1 cells (5,000 cells/well) seeded in 96-well plates. Following a 24 h incubation period, cells were treated with free Dox, Dox@APT_{EDB}-TCL-SPION and Dox@$APT_{scramble}$-TCL-SPION for an additional 2 h. After washing cells with PBS, the medium was replaced with fresh culture medium. At 24 h after the incubation , 10 μl of MTT reagent (5 mg/mL) was added to each well and incubated for 2 h at 37° C. The formazan crystals were solubilized by the addition of 150 μl of DMSO to each well. The optical density at 490 nm was measured and cell viability was determined by the growth curve.

Animal and xenograft tumor model

All animal experiments were approved by the Seoul National University Hospital Biomedical Research Institute Animal Care and Use Committee (IACUC). To develop the tumor model, 2 x 10^6 viable NDY-1 cells were suspended in 0.1 ml matrigel (BD Biosciences) and subcutaneously injected into the back right flank of 4-5 week old BALB/c nude mice. All nanoparticles were suspended in 5% glucose solution for intravenous administration

into tail vein of mice To evaluate EDB-FN targeting images and biodistrubution of APT_{EDB}-TCL-SPION, $APT_{scramble}$-TCL-SPION or TCL-SPION, Eighteen tumor-bearing BALB/c nude mice were randomly assigned to one of 3 experimental groups, with each group containing 6 mice: group 1, APT_{EDB}-TCL-SPION; group 2, $APT_{scramble}$-TCL-SPION; group 3, TCL-SPION. When the tumor volumes were about 200-300 mm^3 at 3 weeks after implantation, mice received a single bolus administration of 20 mg Fe/kg of APT_{EDB}-TCL-SPION, $APT_{scramble}$-TCL-SPION or TCL-SPION via tail-vein injection. To investigate the therapeutic efficacy of Dox@APT_{EDB}-TCL-SPION and Dox@$APT_{scramble}$-TCL-SPION in tumor model, twelve tumor-bearing NOG mice were randomly assigned to one of 3 experimental groups, with each group containing 4 mice: group 1, 5% glucose; group 2, Dox@APT_{EDB}-TCL-SPION; group 3, Dox@$APT_{scramble}$-TCL-SPION. When the tumor volumes were about 150 mm^3 at 2 weeks after implantation, tumor volumes were monitored after three intravenous injections with 2 mg Dox/kg Dox@APT_{EDB}-TCL-SPION, Dox@$APT_{scramble}$-TCL-SPIONs and 5% glucose at 3-day intervals. To determine the volumes of the NDY-1 xenograft tumors, a modified ellipsoidal formula for volume (volume = 1/2[length $\times$ $width^2$]) was used, in which length was the measurement of the greatest longitudinal diameter and width was the greatest transverse diameter. MRI

studies were performed, all tumors were isolated and histological analyses of tumors were performed.

In vitro MRI

Transverse relaxivities of TCL-SPION, APT_{EDB}-TCL-SPION and $APT_{scramble}$-TCL-SPION were evaluated using a spin echo sequence on a 3 Tesla clinical MR scanner (Magnetom Trio; Siemens Healthcare, Erlangen, Germany). For measurements of R_2 ($1/T_2$) values, nanoparticles dispersed in water were prepared and multiecho T_2-weighted images were acquired using the following parameters: repetition time (TR) 5000 msec; Flip angle = 90 ° ; echo delay time (TE) = 16, 32, 48, 64 msec and, 20,40,60,80 msec; bandwidth = 310 Hz/pixel; matrix = 320x320, field of view (FOV) = 100x90 mm, number of excitations (NEX)=1. T_2 values were calculated by a linear fit of the logarithmic signal amplitudes versus TE. For measurements of T_2 values from cell phantoms, MCF-7 and NDY-1 cells were seeded at a density of 2×10^6 cells / well in 100 mm tissue culture plates and incubated for 2 days. After free APT_{EDB} (0.1 mg/ml) blocking for 1 h, and then cells were treated with APT_{EDB}-TCL-SPION or $APT_{scramble}$-TCL-SPION (iron concentration, 11.2 μg Fe/ml) for 2 h, 4 h and 12 h. Following a incubation under 5% CO_2 at 37◦C, the cells were collected, washed, and dispersed in PBS. Multiecho T_2-weighted images of the

collected cells were obtained and T_2 values measured as described in the previous section.

In vivo MRI

When the average tumor volume reached to 200–300 mm^3, *in vivo* MRI studies were performed with a human wrist coil on a 3.0 T clinical MR scanner (Magnetom Trio, Siemens Healthcare). For whole–animal MRI, mice were anesthetized with isofluorane (1% in 100% oxygen). To stabilize the body temperature of the mice during MRI experiments, an animal warming system (Agilent, Santa Clara, CA, USA) which consists of a warm water (39 ° C) reservoir with a pump and hoses placed underneath the animal bed was used. Pre–MR images were obtained before injection with nanoparticles, and longitudinal follow–up MR images were obtained 4 h and 24 h after intravenous injection of APT_{EDB}–TCL–SPION and $APT_{scramble}$–TCL–SPION. Post–treatment MR images of tumors were obtained 1 day, 4 day, 7 day after intravenous injection of Dox@APT_{EDB}–TCL–SPION and Dox@$APT_{scramble}$–TCL–SPION. T_2*–weighted images were obtained using a gradient echo sequence (TR/TE = 40/22 ms, FOV = 40 × 80 mm2, flip angle = 15° , matrix size = 256 × 128, NEX = 3, number of slices = 24, and section thickness = 0.8 mm). To determine the signal intensity (SI) changes in the T_2*–weighted images of the liver, spleen,

kidney, and thigh muscles, regions of interest (ROI) were manually drawn to outline the outer boundaries of the organs. In addition, ROIs of the tumor were drawn just inside the outer margins of each tumor in the T_2*-weighted images to avoid placing the ROIs over artifacts at the tissue-air interface. The SI changes were analyzed from all-slice images of each tumor and were subsequently defined as the tumor SI. For the quantitative analysis of the signal intensity changes induced by the accumulation of SPIONs in tumors, signal intensities from the muscle was used as a reference to calibrate the ROI signal in the tumors [26, 27]. The ratio of the SI changes for tumor versus muscle was calculated both prior to and after the injection of TCL-SPION, APT_{EDB}-TCL-SPION or $APT_{scramble}$-TCL-SPION according to the following formula: SI ratio = [SI tumor (post)) / SI muscle (post)] / [SI tumor (pre) / SI muscle (pre)]. The results of the *in vivo* MRI were analyzed by observing the differences between pre- and post-contrast SI.

Histological analysis

After MRI examination, the histological analysis of the several tissues (brain, heart, liver, spleen, kidney and thigh muscle) and tumors of mice was performed. The tumor and tissues were removed at 24 h post-injection of APT_{EDB}-TCL-SPION or $APT_{scramble}$-TCL-SPION. The excised tissues were fixed with 10%

buffered formalin and embedded in paraffin blocks. Tissues were sectioned into 4-μm-thick sections. Hematoxylin and eosin (H&E) staining was performed to distinguish between the viable and nonviable cell populations within the tissues. The presence of APT_{EDB}-TCL-SPION and $APT_{scramble}$-TCL-SPION in each section was detected using Prussian blue staining which stains the ferric irons. In brief, sectioned tissues were incubated for 60 minutes with 10% potassium ferrocyanide (Sigma) in 10% hydrochloric acid, then rewashed and counterstained with nuclear fast red (Sigma) for 7 minutes. The EDB-FN protein expression and distribution of the vascular endothelium in tumors were investigated by immunostaining using antibodies for BC-1 (Santa Cruz Biotechnology, Inc. Dallas, Texas, USA) and CD31 (Abcam, Cambridge, MA, USA) with the appropriate secondary antibody; tissue sections were stained with diaminobenzidine solution (Dako, Hamburg, Germany) for 2-5 minutes. Histological images of stained tissues were acquired with a microscopy (Leica, Wetzlar, Germany), equipped with a CCD camera (Leica).

Statistical analysis

The means ± standard deviations were calculated from at least three independent experiments and statistically evaluated using a one-way ANOVA model followed by the Student-Newman-Keuls

test. For all tests, a p-value less than 0.05 was considered statistically significant.

RESULTS

Assessment of EDB-FN expression in BTIC and differentiated breast cancer cells. Using RT-PCR, flow cytometry and immunostaining, the expression levels of BTIC-characteristic genes related to self-renewal (Nanog, Oct4, and KLF4), surface marker genes (CD44 and CD24) and a putative gene (ALDH1) were analyzed in NDY-1 and MCF-7 cells (representing BTIC and differentiated breast cancer cells, respectively). As expected, NDY-1 cells exhibited a phenotype associated with BTICs, showing a high expression of CD44 and ALDH1A1-3 but little expression of CD24 (Figure 1A). Moreover, expression of self-renewal genes that are characteristic markers of stem cells was also evident in NDY-1 cells. Flow cytometric analysis confirmed the expression of CD44 and CD24 markers (Figure 1B). For analysis of the putative BTIC marker, ALDH activity was assessed using an ALDEFLUOR assay in the presence and absence of ALDH inhibitor, DEAB. Approximately 26% of NDY-1 cells stained positively with ALDEFLUOR (Figure 1C); representative immunostaining of ALDH1 showed high expression of ALDH1 proteins in the NDY-1 spheroid (Figure 1C).

Once we confirmed the expression of BTIC-characteristic genes in NDY-1 cells, EDB-FN expression in diverse breast cancer cell lines such as SUM-225, MCF-7, BT-474, MDA-MB-231 and NDY-1 was examined using RT-PCR. Interestingly, abundant expression of EDB-FN mRNA was observed in NDY-1 cells as compared with the other breast cancer cells (Figure 2A). Furthermore, the expression of EDB-FN in NDY-1 cells was then examined using both an EDB-FN specific antibody (BC-1) and a dye-labeled EDB-FN specific aptide . The aptide fluorescence signal (shown in red) was observed in NDY-1 cells but not MCF-7 cells, which do not express EDB-FN (Figure 2B). The signal co-localized with the areas immunostained by the BC-1 antibody. NDY-1 cells expressed BTIC-characteristic genes as well as high-levels of EDB-FN, which may be a new biomarker for identifying BTICs.

To determine the function of EDB-FN in NDY-1 cells, EDB-FN was specifically downregulated by treatment with EDB-FN siRNA and the levels of expression of BTIC-associated genes assayed by RT-PCR. This specific siRNA achieved effective EDB-FN knockdown 72 h after transfection (Figure 3A). This EDB-FN knockdown led to downregulation of expression of CD44 and ALDH1, both characteristic markers of BTICs (Figure 3A), as well

as of genes related to self-renewal capacities (KLF-4, c-Myc, Oct-4 and Nanog) (Figure 3B). In addition, genes related to the epithelial-mesenchymal transition (EMT) (N-cadherin, Slug and Twist) and drug resistance (ABCG-2) were substantially downregulated by EDB-FN siRNA (Figure 3C). Flow cytometry analysis showed that the percentage of CD44+/CD24- cells was lower in EDB-FN knockdown than in normal cells (91% vs 95%; Figure 3D).

The schematic illustration for the preparation of APT_{EDB}-TCL-SPION is shown in Figure 4A. As reported previously, aptides form unique pre-organized structures consisting of robust -hairpin structures in the middle (shown in green) and variable amino acid chains at both the N- and C-termini (shown in red and blue, respectively), which are responsible for target binding (Figure 4B) . To facilitate conjugation, we used a slightly modified APT_{EDB}, containing an additional cysteine residue at the lysine site of the hairpin scaffold region, as indicated in Figure 4B[20]. The hydrodynamic size and zeta potential of TCL-SPION, Mal-TCL-SPION and APT_{EDB}-TCL-SPION were measured by dynamic light scattering (data not shown). As expected, the size of TCL-SPION (34.7 ± 10.9 nm) increased with attachment of Mal-PEG_{1000} (36.1 ± 10.8 nm) and then the aptide (38.1 ± 11.8 nm). Also, there was

distinct change in the zeta potential of each nanoparticle (−29.2 for TCL−SPION *versus* −36.6 for APT_{EDB}−TCL−SPION). The size increase and change in zeta potential from the bare TCL−SPION suggest the successful conjugation of the aptide.

The transverse relaxation time (T_2) of protons in a water solution of each SPION was measured using a 3 Tesla clinical MRI and the specific relaxivity from the change in the relaxation rate (R_2) was derived at various iron oxide concentrations. The dark signals on the T_2−weighted MR images of APT_{EDB}−TCL−SPION, $APT_{scramble}$−TCL−SPION and TCL−SPION were gradually increased in a dose−dependent manner (Figure 5A); three SPIONs showed relaxivity of 232.1 ± 1.4 $mM^{-1}sec^{-1}$ for APT_{EDB}−TCL−SPION, 211.1 ± 2.1 $mM^{-1}sec^{-1}$ for $APT_{scramble}$−TCL−SPION, and 259.89 ± 3.2 $mM^{-1}sec^{-1}$ for TCL−SPION (Figure 5B).

We next examined whether APT_{EDB}−TCL−SPION could specifically bind to BTICs (NDY−1 cells) using *in vitro* MRI of cell phantoms. NDY−1 and MCF−7 cells were incubated with APT_{EDB}−TCL−SPION or $APT_{scramble}$−TCL−SPION at a concentration of 11.2 μg Fe/ml for 2 h, 4 h and 12 h. To confirm the APT_{EDB}−TCL−SPION exhibit specific reaction between the APT_{EDB} and EDB−FN in NDY−1 cells, the blocking reaction with free APT_{EDB} (0.1mg/ml)

was performed for 1 h before the treatment with APT_{EDB}-TCL-SPION. A representative MRI phantom image showed a clear dark signal only in NDY-1 cells incubated with APT_{EDB}-TCL-SPION for 12 h (Figure 6A). There was a significant difference in the T_2 values measured from T_2-weighted MRI of the NDY-1 cell phantom between the APT_{EDB}-TCL-SPION and $APT_{scramble}$-TCL-SPION (Figure 6B, $*p<0.05$). The free EDB-FN aptides blocking prevented the binding affinity of APT_{EDB}-TCL-SPION, resulting in inhibition of decreased T_2 values of NDY-1 cells incubated with APT_{EDB}-TCL-SPION for 12 h (Figure 6B). Only marginal decreases in the signal intensity and T_2 values measured from T_2-weighted MR images were observed but were not significant in EDB-FN negative MCF-7 cells after treatment with both APT_{EDB}-TCL-SPION and $APT_{scramble}$-TCL-SPION.

We carried out the additional *in vitro* MRI of cell phantoms at different cell number to evaluate the sufficiently sensitive for EDB-FN targeted BTIC imaging using APT_{EDB}-TCL-SPIONs. At $5x10^5$ BTICs were detected by EDB-FN targeted MRI using APT_{EDB}-TCL-SPIONs on 3T clinical MR scanner (Figure 7A and B).

To examine the feasibility of APT_{EDB}-TCL-SPION as a targeted MRI contrast agent *in vivo*, we prepared NDY-1 tumors in

mice to model EDB-FN positive BTICs-derived tumors. After intravenous injection of APT_{EDB}-TCL-SPION and $APT_{scramble}$-TCL-SPION at a dose of 20 mg Fe/kg in a 5% glucose solution, *in vivo* tumor MR images were obtained before and after injection of APT_{EDB}-TCL-SPION and $APT_{scramble}$-TCL-SPION. Figure 8 shows representative T_2*-weighted MR images of tumors selected from each group mice (n=6). At 4 h and 24 h post-injection of APT_{EDB}-TCL-SPION, dark signals were clearly detected on the serial T_2*-weighted MR images of tumor (Figure 8). For quantitative measurement of SI changes and exclusion of the substantial artifact at tissue-air interface in the subcutaneous tumor, ROIs were manually drawn just inside the outer margins of T_2*-weighted MR images of each tumor and SI changes were analyzed from all-slice MRIs of each tumor (Figure 9). The SI change between the post- and pre-MR images of tumors of mice injected with APT_{EDB}-TCL-SPION was significantly different at 4h and 24 h (Figure 10, $*p<0.05$). However, only marginal changes in the dark signal and signal intensity within the tumor were observed after $APT_{scramble}$-TCL-SPION and TCL-SPION injection (Figure 10 and 11). Liver and spleen exhibited relatively big changes in signal intensity as compared with tumors (Figure 10). The immediately enhanced contrast effect disappeared in kidney at 1 h post-injection and the change in signal intensities measured from MR images of brain and

thigh muscle was no detected after APT_{EDB}-TCL-SPION and $APT_{scramble}$-TCL-SPION injection (data not shown).

In order to evaluate and confirm the accumulation and distribution of intravenously administered APT_{EDB}-TCL-SPION and $APT_{scramble}$-TCL-SPION within tumor as well as several tissues (brain, liver, spleen, kidney and thigh muscle), Prussian blue staining of tissues isolated from mice at 24 h post-injection of APT_{EDB}-TCL-SPION and $APT_{scramble}$-TCL-SPION was performed. Blue dots representing stained iron particles were not detected in sections of brain, heart, kidney and muscle but many blot dots were observed liver and spleen of mice injected with APT_{EDB}-TCL-SPION or $APT_{scramble}$-TCL-SPION, which indicates nanoparticles preferentially distribute to spleen and liver regardless of their conjugation of a target-specific ligand conjugation with (Figure 12).

To investigate the histological change such as necrotic region within tumors of mice injected with APT_{EDB}-TCL-SPION and $APT_{scramble}$-TCL-SPION, H&E staining was performed. Necrotic area was no detected in APT_{EDB}-TCL-SPION-tumor or $APT_{scramble}$-TCL-SPION-tumor sections (Figure 13, upper). Next we evaluated the presence of APT_{EDB}-TCL-SPION or $APT_{scramble}$-TCL-SPION within tumor section (Figure 13, middle). As expected,

a large number of the blue dots was observed in the sectioned tumor of mice injected with APT_{EDB}-TCL-SPION. In contrast, many fewer nanoparticles were detected in the $APT_{scramble}$-TCL-SPION-tumor. We further performed the immunohistological analysis with the anti-EDB-FN antibody (BC-1) to compare with EDB-FN expression level between APT_{EDB}-TCL-SPION-tumor and $APT_{scramble}$-TCL-SPION-tumor. A high-level of EDB-FN expression was observed in the APT_{EDB}-TCL-SPION- or $APT_{scramble}$-TCL-SPION-tumor section (Figure 13, lower).

To investigate the vascularity of the APT_{EDB}-TCL-SPION-tumor, endothelial cell marker was stained with anti-CD31 antibody. Figure 14A showed a large number of vessels in the extracellular matrix of the interstitial space of the APT_{EDB}-TCL-SPION-tumor section. Furthermore, co-staining with anti-EDB-FN antibody and Prussian blue in APT_{EDB}-TCL-SPION-tumors revealed that APT_{EDB}-TCL-SPIONs were mainly distributed in the EDB-FN positive extracellular matrix of the interstitial space exhibiting a highly vascular structure (Figure 14B).

The therapeutic efficacy of targeted nanoparticles was then evaluated by treating NDY-1 cells with Dox@APT_{EDB}-TCL-SPION , Dox@$APT_{scramble}$-TCL-SPIONs or free Dox. As shown in

Figure 15A and B, The cytotoxicity of Dox@APT_{EDB}-TCL-SPION against NDY-1 cells was significantly comparable to that of Dox@$APT_{scramble}$-TCL-SPIONs and free Dox.

To examine *in vivo* therapeutic efficacy, inhibition of tumor growth in a NDY-1 xenograft mouse model was evaluated. As shown in Figure 16, tumor growth was remarkably inhibited in the Dox@APT_{EDB}-TCL-SPION-treated group, which exhibited a significant decrease in tumor volumes compared to those of Dox@$APT_{scramble}$-TCL-SPIONs-treated groups and untreated groups ($* P < 0.05$). There were no significant differences between the body weights of treated and untreated mice, suggesting the absence of physical distress over the course of the experiment (data not shown).

DISCUSSION

Current therapies such as a combination of surgery, chemotherapy, hormone therapy, and radiation therapy can eliminate the bulk of a breast tumor, but they fail to completely eradicate the BTICs responsible for the recurrence and metastasis of the cancers [28]. Therefore, screening and identifying characteristic BTIC biomarkers is important for distinguishing BTICs from differentiated tumor cells within the tumor mass. It has been shown that the BTICs found in breast cancer express characteristic biomarkers (CD44+/CD24−/ALDH1+) that are distinct from differentiated breast cancer cells [1, 4]. In this study, we found that NDY−1 cells, which are derived from the cancerous tissue of a breast cancer patient, highly expressed the self−renewal genes Oct−4, Nanog, and KLF4 in addition to the characteristic biomarkers of BTICs. We also observed that NDY−1 cells specifically expressed abundant EDB−FN and selective EDB−FN knockdown using siRNA markedly suppressed the mammosphere−forming ability of these cells(data not shown), as well as their expression of BTIC markers (CD44, ALDH1), self−renewal−related genes (KLF−4, c−Myc, Oct−4, Nanog), a drug−resistance−related gene (ABCG−2) and EMT markers (N−cadherin, Slug, Twist). To the best of our knowledge, this is the first report to

document the relationship between EDB-FN expression and BTICs.

For the *in vivo* imaging studies using EDB-FN positive tumors in preclinical and clinical trials, EDB-FN specific antibodies or peptides labeled with fluorescent dyes or a radioisotope were examined using an optical system, positron electron tomography (PET), and single-photon emission computed tomography (SPECT) [7, 29, 30]. Antibodies have been widely used in the development of specifically targeted imaging probes due to their intrinsic high affinities and specificities; however, their large size is a primary cause of insufficient tissue penetration, which results in poor image quality [31, 32]. Therefore, alternatives to antibodies and the development of active biomarker conjugated-imaging probes are required for the specific diagnosis and treatment of tumors [13, 14, 33, 34]. Our previous studies have shown that the small size high-affinity peptide aptide (APT_{EDB}) can easily extravasate and specifically bind to EDB-FN as a targeting ligand for the delivery of a drug-encapsulating liposome for cancer therapy [22]. To allow the selective detection of EDB-FN-expressing tumors via *in vivo* MRI, we recently synthesized oleic acid-stabilized SPIONs by conjugating them with APT_{EDB} [21]. Previous reports have considered APT_{EDB} a desirable moiety for the selective and effective detection of EDB-FN. Furthermore, APT_{EDB}-conjugated nanoparticles can be useful for specific drug delivery and *in vivo*

imaging by MRI of EDB-FN expressing tumors located in deep tissues.

Optical imaging reporter genes can visualize BTICs in the xenograft of living animals [3]. However, *in vivo* optical imaging has limited tissue penetration and the disadvantage of low spatial resolution. MRI can provide tomographic or volumetric imaging of internal organs at high anatomical resolutions and soft tissue contrast without using ionizing radiation, which is not possible using other imaging modalities. MRI has the potential to become a valuable imaging modality to accurately evaluate the response to chemotherapy and to determine whether to use surgery or irradiation for local tumor control [35]. We demonstrated that tagging BTICs with an MRI reporter is able to distinguish between dead and live BTICs within a tumor after chemotherapy [25]. Cell surface markers such as CD44 have been used to target BTICs and other TICs using hyaluronic acid (HA)-modified nanoparticles [36]; however, CD44 is expressed ubiquitously in a large number of mammalian cell types, including differentiated cancer cells. Because of the specific and high expression of EDB-FN in BTICs, we assume here that EDB-FN is the most reliable biomarker to selectively target and image BTICs. The development of EDB-FN ligand-conjugated SPIONs could provide information regarding the

biological characteristics of individual tumors before and after treatment and an opportunity to test new targeted treatments of BTICs. The use of APT_{EDB}-TCL-SPION as an MRI contrast agent exhibits a much higher transverse relaxivity than the oleic acid SPION (230 mM-1 sec-1 versus 120 mM-1 sec-1) [21]. This implies that APT_{EDB}-TCL-SPIONs can be utilized for the efficient EDB-FN targeted MRI at low concentrations, which may result in the reduction of harmful effects generated by the SPIONs. BTICs are thought to be a small population of cells with self-renewal capacity and therapeutic resistance in tumors [1]. Therefore, studies validating that MRI is sufficiently sensitive and suitable for the detection of the low population numbers of BTICs in the tumor may be critical. Our previous study showed that the viable CD44+/CD24- populations of BTICs within the tumor after chemotherapy can be quantitatively analyzed by non-invasive MRI [25]. The present study demonstrates that at least 5×10^5 BTICs were sufficient for detection using this method and that BTICs within the tumor mass could be clearly detected using APT_{EDB}-TCL-SPIONs and a 3T clinical MR scanner. We suggest that MRI using APT_{EDB}-TCL-SPIONs is sufficiently sensitive and suitable for EDB-FN targeted imaging of BTICs. Furthermore, anticancer drugs such as doxorubicin can easily be loaded in the polymeric shell of the APT_{EDB}-TCL-SPION to construct a theranostic system

for combined cancer imaging and therapy of BTICs, as shown in our previous studies [18, 19]. The use of clinically applicable higher-field 7T MRI scanners and more sensitive susceptibility- weighted imaging sequences would improve the detection sensitivity of BTICs using APT_{EDB}-TCL-SPION. EDB-FN targeted MRI has the potential to be used in clinical practice to identify and localize BTICs within the tumor mass before surgery and to monitor the response to treatment in breast cancer [37].

In conclusion, we report, for the first time, that EDB-FN is highly expressed in BTICs but not in differentiated breast cancer cells, suggesting that EDB-FN can be used as a new characteristic biomarker for identifying BTICs. Furthermore, we developed an imaging probe targeting BTICs, which was constructed by covalently attaching EDB-FN specific high-affinity peptide to TCL-SPION and enabled visualization of BTIC tumors in vivo by MRI. Furthermore, Dox@APT_{EDB}-TCL-SPION showed the successful therapeutic effects by selective and efficient drug-delivery in the xenograft mouse model. The exceptional, active tumor-targeting ability of Dox@APT_{EDB}-TCL-SPION allows for simultaneous detection of EDB-FN positive BTIC tumors by MRI, delivery of anti-cancer drugs to the tumor sites, and monitoring of therapeutic responses of tumors. In the near future, we will study

the therapeutic feasibility of APT_{EDB}-TCL-SPION combined with therapeutic drugs and EDB-FN RNAi as a novel theranostic system that allows for simultaneous diagnosis and therapy of hard-to-treat BTICs in breast cancers.

TABLE AND FIGURE

Table 1. Specific primer sequences for RT-PCR to detect the self-renewal genes and marker gene expression in breast tumor initiating cells

Primer	Sequence	Size (bp)
CD44	(forward)5'-TCCAACACCTCCCAGTATGACA-3' (reverse)5'-GGCAGGTCTGTGACTGATGTACA-3'	60
CD24	(forward)5'-TATTTGGGAAGTGAAGACTGGAA-3' (reverse)5'-TCTAAATGTGGCTATTCTGATCCA-3'	96
ALDH1A1	(forward)5'-TGTTAGCTGATGCCGACTTG-3' (reverse)5'-TTCTTAGCCCGCTCAACACT-3'	135
ALDH1A2	(forward)5'-CTGGCAATAGTTCGGCTCTC-3' (reverse)5'-TGATCCTGCAAACACTGCTC-3'	130
ALDH1A3	(forward)5'-TCTCGACAAAGCCCTGAAGT-3' (reverse)5'-TATTCGGCCAAAGCGTATTC-3'	130
KLF-4	(forward)5'-TATGACCCACACTGCCAGAA-3' (reverse)5'-TGGGAACTTGACCATGATTG-3'	90
c-Myc	(forward)5'-CGGAACTCTTGTGCGTAAGG-3' (forward)5'-CTCAGCCAAGGTTGTGAGGT-3'	104
Oct-4	(forward)5'-ACCGAGTGAGAGGCAACC-3' (reverse)5'-TGAGAAAGGAGACCCAGCAG-3'	183
Nanog	(forward)5'-CCTGTGATTTGTGGGCCTG-3' (reverse)5'-GACAGTCTCCGTGTGAGGCAT-3'	200
EDB-FN	(forward)5'-CCAGGTACAGGGTGACCTAC-3' (reverse)5'-CTCTCCATATCATCGTGCAA-3'	154
N-cadherin	(forward)5'-CTCCTATGAGTGGAACAGGAACG-3' (reverse)5'-TTGGATCAATGTCATAATCAAGTGCTGTA-3'	149
Twist	(forward)5'-GGAGTCCGCAGTCTTACGAG-3' (reverse)5'-TCTGGAGGACCTGGTAGAGG-3'	161
Slug	(forward)5'-TTTCTGGGCTGGCCAAACATAAGC-3' (reverse)5'-ACACAAGGTAATGTGTGGGTCCGA-3'	139
ABCG-2	(forward)5'-GGATGAGCCTACAACTGGCTT-3' (reverse)5'-CTTCCTGAGGCCAATAAGGTG-3'	181
β-actin	(forward)5'-ATCATGTTTGAGACCTTCAA-3' (reverse)5'-CATCTCTTGCTCGAAGTCCA-3'	208

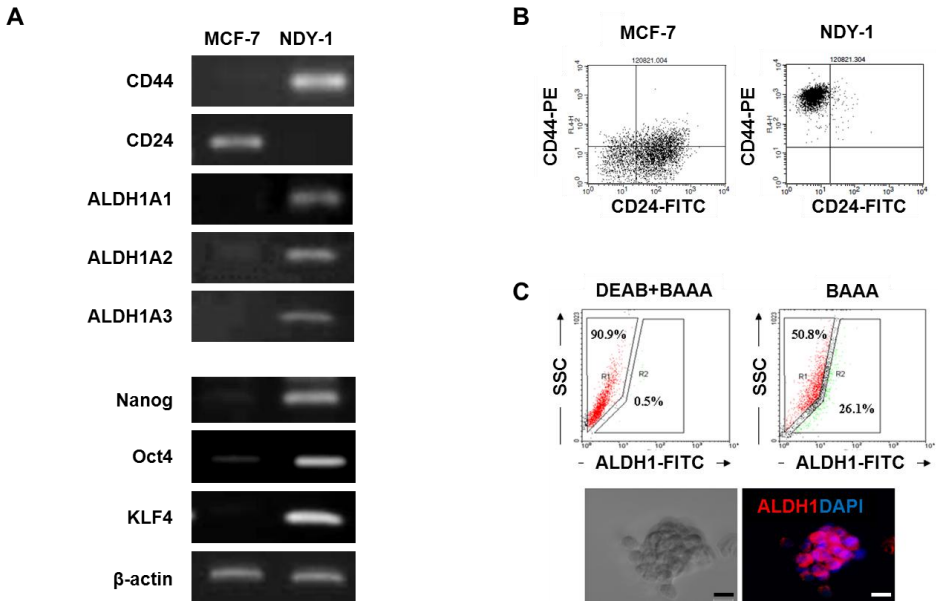

Figure 1 : Analysis of the genes expressed in breast tumor initiating cells (BTICs). (A) RT-PCR analysis of the self-renewal genes(Nanog, Oct4, KLF4) and surface marker genes (CD44+/CD24-/ALDHhigh) in BTICs (NDY-1) and breast cancer cells (MCF-7). Specific marker of BTICs and self-renewal genes were highly expressed in NDY-1 cells but not MCF-7 cells. (B) Flow cytometric analysis of the surface markers CD44 and CD24. NDY-1 exhibited a CD44+/CD24- BTIC phenotype. (C) ALDEFLUOR assay for ALDH1 activity and Immunostaining analysis for ALDH1 expression. Approximately 26% of NDY-1 cells exhibited brightly fluorescent ALDH1 staining, indicating the

putative BTIC marker. Immunostaining showed NDY-1 spheroids strongly express the ALDH1 protein. Scale bar: 20 μm

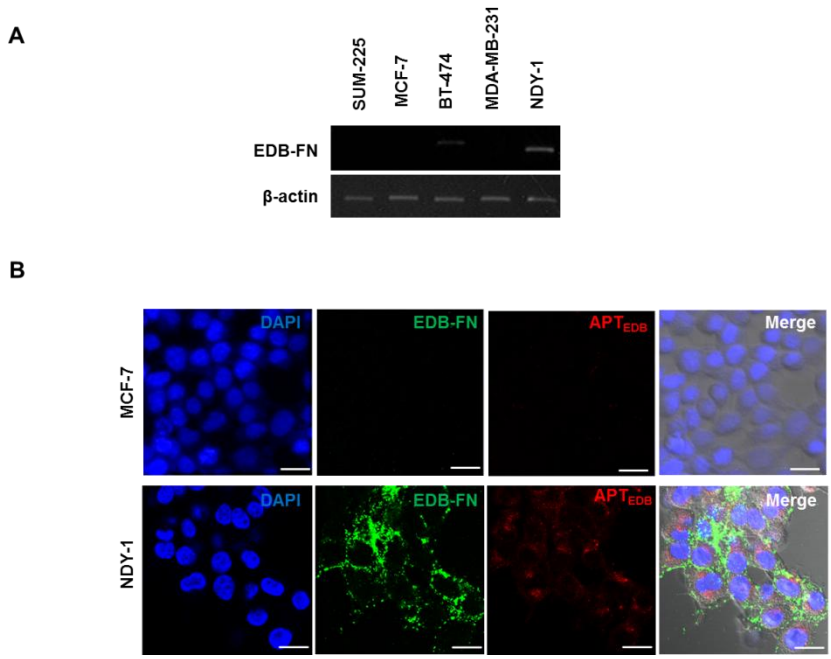

Figure 2: Analysis of the extra domain-B of fibronectin (EDB-FN) and selective targeting with an EDB-FN aptide (APT_{EDB}). (A) RT-PCR analysis of the EDB-FN mRNA in diverse breast cancer cell lines. EDB-FN was expressed in NDY-1 cells but not SUM-225, MCF-7, BT-474, and MDA-MB-231 cells. (B) EDB-FN targeted images of the Cy3.3-labeled APT_{EDB} (Cy3.3-APT_{EDB}, red fluorescence) and immunostained images of EDB-FN (green fluorescence) in breast cancer cells. Cy3.3-APT_{EDB} specific signals were observed in EDB-FN overexpressing NDY-1 cells not but MCF-7 cells. Scale bar: 20 μm

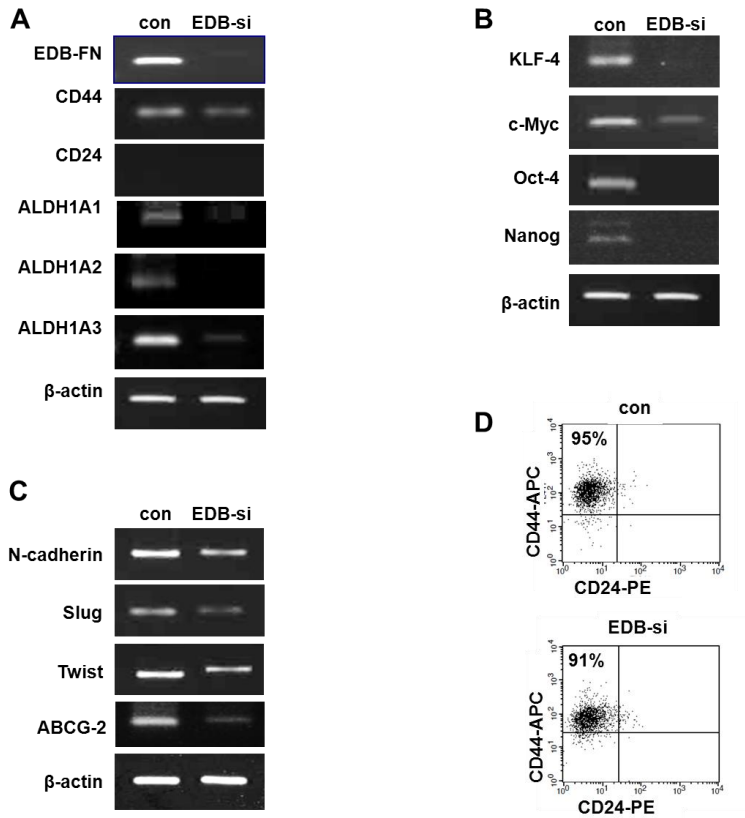

Figure 3: Decreased expression of genes associated with breast tumor initiating cell (BTIC) markers, self-renewal capacity, epithelial-mesenchymal transition (EMT) and drug-resistance in EDB-FN-knockdown NDY-1 cells. (A-C) RT-PCR analysis of genes associated with BTIC markers (CD44, CD24, and ALDH1A), self-renewal (KLF-4, c-Myc, Oct-4 and Nanog), EMT (N-cadherin, Slug and Twist) and drug-resistance (ABCG-2). Specific EDB-FN siRNA strongly silenced EDB-FN expression, as well as

suppressing the expression of CD44, ALDH1A1-3, KLF-4, c-Myc, Oct-4, Nanog, N-cadherin, Slug, Twist and ABCG-2 mRNAs in BTICs. (D) Flow cytometry analysis of EDB-FN knockdown cells.

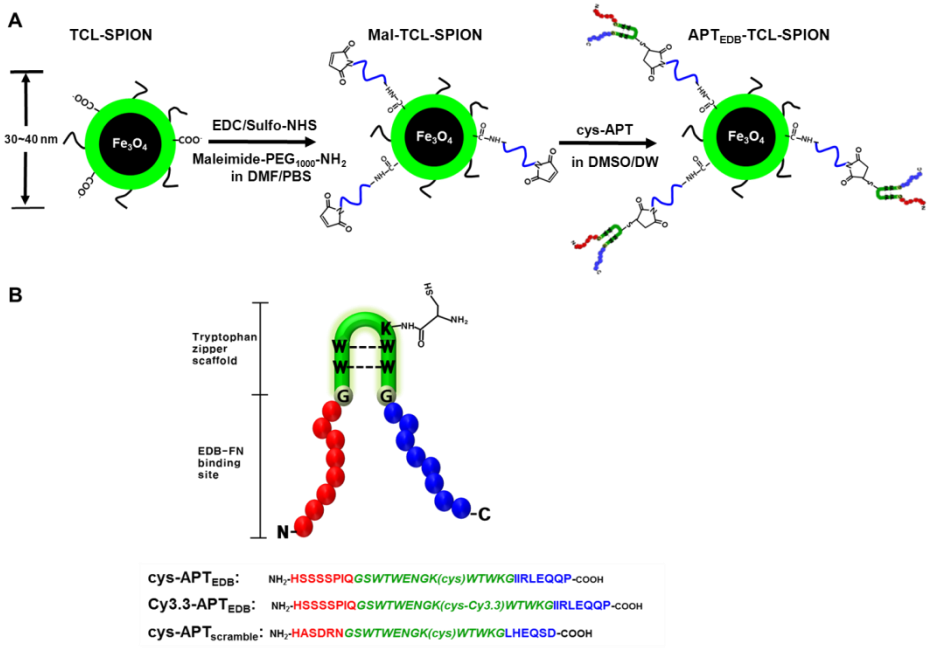

Figure 4: (A) Schematic representation of the preparation and characterization of EDB-FN aptide (APT_{EDB})-conjugated SPION. (B) Schematic of the principal features of EDB-FN aptide (APT_{EDB}).

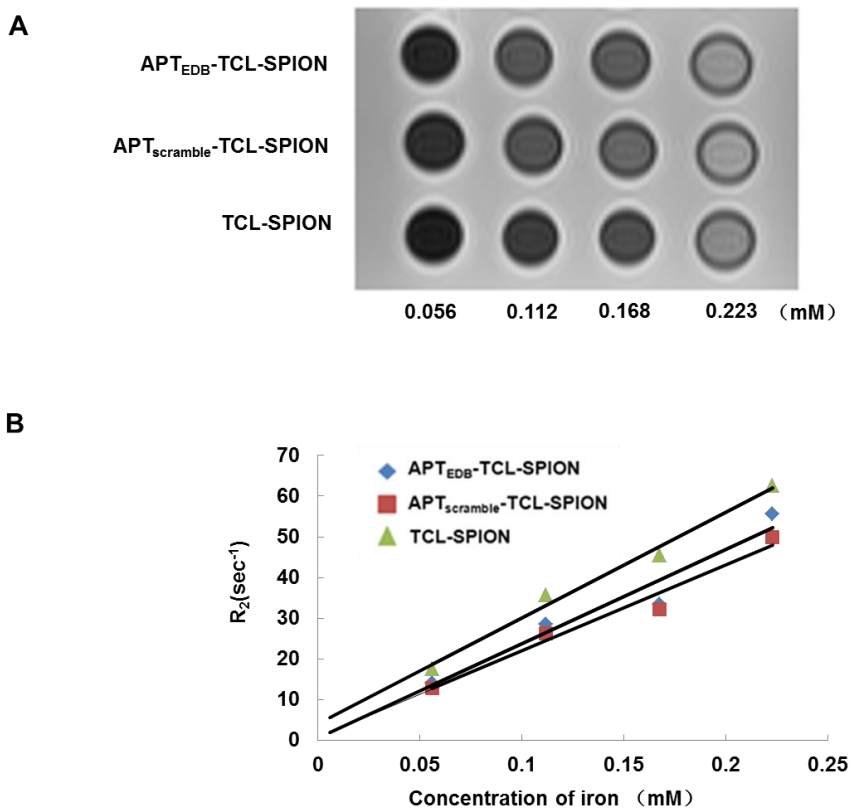

Figure 5: Comparison of magnetic properties. A: T_2-weighted MRI and plots of the relaxation rate (R_2 value) of APT_{EDB}-TCL-SPION, $APT_{scramble}$-TCL-SPION, and TCL-SPION at various iron concentrations. B: The transverse relaxivity of APT_{EDB}-TCL-SPION, $APT_{scramble}$-TCL-SPION and TCL-SPION were 232.1 ± 1.4mM^{-1} sec^{-1}, 211.1± 2.1mM^{-1} sec^{-1} and 259.9 ± 3.2mM^{-1} sec^{-1}, respectively.

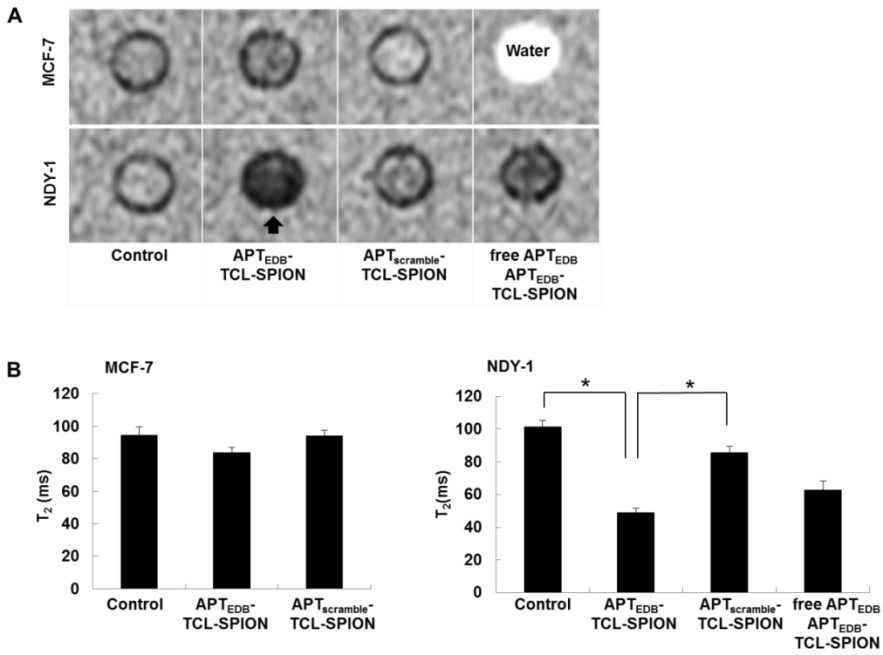

Figure 6: ***In vitro*** **MRI analysis of cell phantoms.** (A) Representative T_2-weighted MRI of cell phantoms. Cells were treated with APT_{EDB}-TCL-SPION and $APT_{scramble}$-TCL-SPION (11.2 μg Fe/ml) for 12 h at 37° C. Blocking of specific binding of APT_{EDB}-TCL-SPION was achieved by pretreatment with EDB-FN aptide (APT_{EDB}, 0.1 mg/ml) for 1 h. Dark signals (arrow) were clearly detected in NDY-1 cells treated with APT_{EDB}-TCL-SPION. (B) T_2 values measured from the T_2-weighted MRI of cell phantoms. T_2 values significantly decreased in the APT_{EDB}-TCL-SPION-treated NDY-1 cells compared with APT_{EDB}-TCL-SPION-treated NDY-1 or untreated controls. The significantly

different T_2 values were not observed in APT_{EDB}-TCL-SPION and $APT_{scramble}$-TCL-SPION labeled MCF-7 cells and untreated controls. Preincubation with free APT_{EDB} inhibited the decrease in T_2 values of APT_{EDB}-TCL-SPION-treated NDY-1 cells. All values are presented as the mean ± standard deviation of at least three independent experiments. Asterisks (*) point out that *P* value was statistically significant (<0.05).

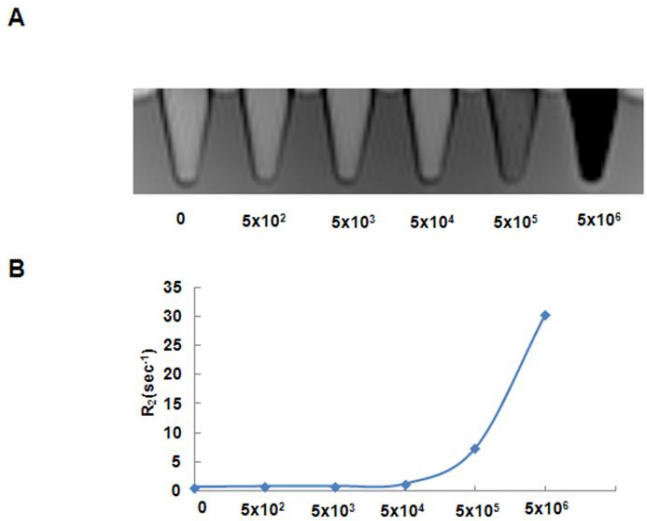

Figure 7: *In vitro* MRI of cell phantoms at different cell number. A and B: At $5x10^5$ BTICs were detected by EDB-FN targeted MRI using APT_{EDB}-TCL-SPIONs on 3T clinical MR scanner.

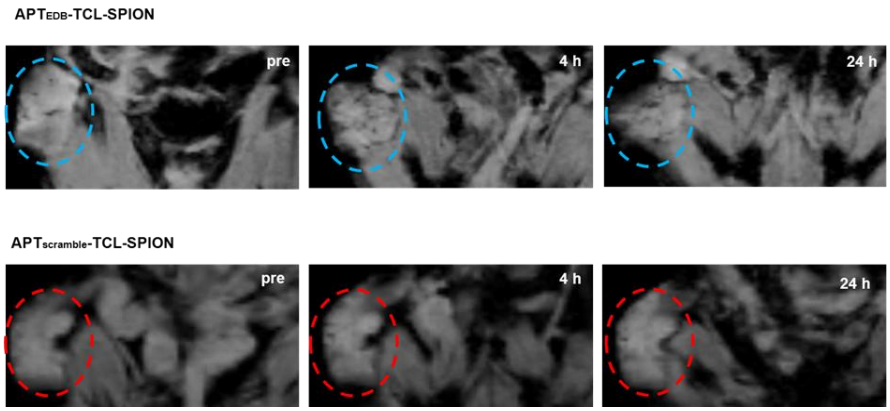

Figure 8: ***In vivo*** **EDB-FN targeted tumor MRI.** T_2*-weighted MRI of the NDY-1 tumor. Serial follow-up MRI of the tumor on the right side of the mouse was performed before and after the injection of APT_{EDB}-TCL-SPION or $APT_{scramble}$-TCL-SPION (20 mg Fe/kg). The circles indicate the engrafted tumor region. Dark signals were observed in tumors of mice injected with APT_{EDB}-TCL-SPION.

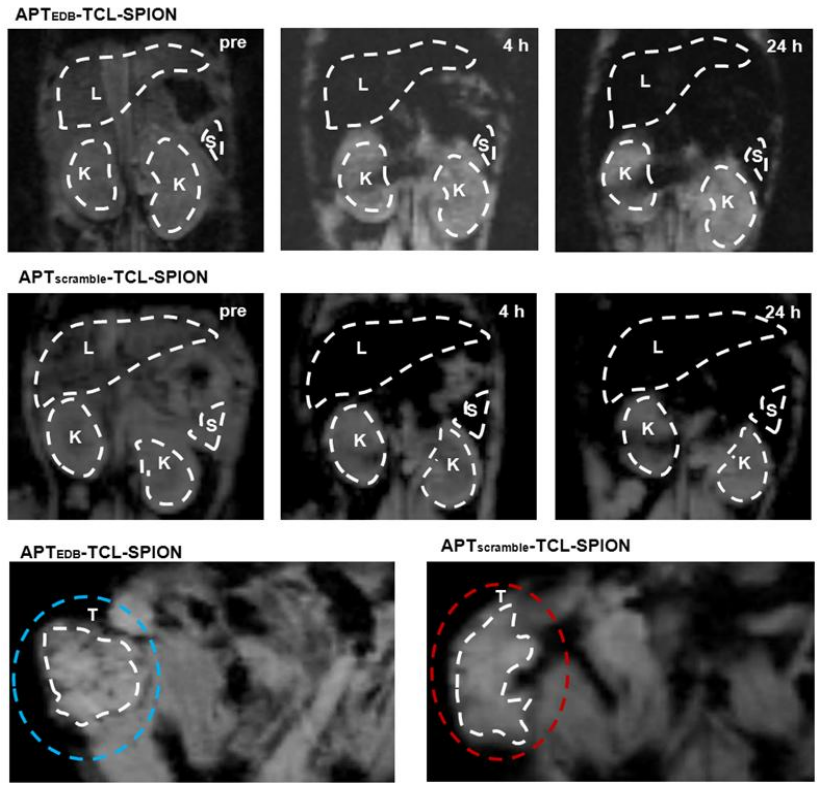

Figure 9: T_2*-weighted images showing ROIs drawn in tumor, liver, spleen and kidney areas of mice injected with APT_{EDB}-TCL-SPION and $APT_{scramble}$-TCL-SPION. Representative T_2*-weighted MRIs of tumor, liver, spleen and kidney. ROIs were drawn just inside the outer margins of the tumor (T), liver (L), spleen (S) and kidney (K) as shown in T_2*-weighted MRIs. Liver and spleen exhibited relatively big changes in signal intensity as compared with tumors,

Tumor: T, Liver: L, Spleen:S, Kidney: K, Dot line : tissue area, Circule: ROI.

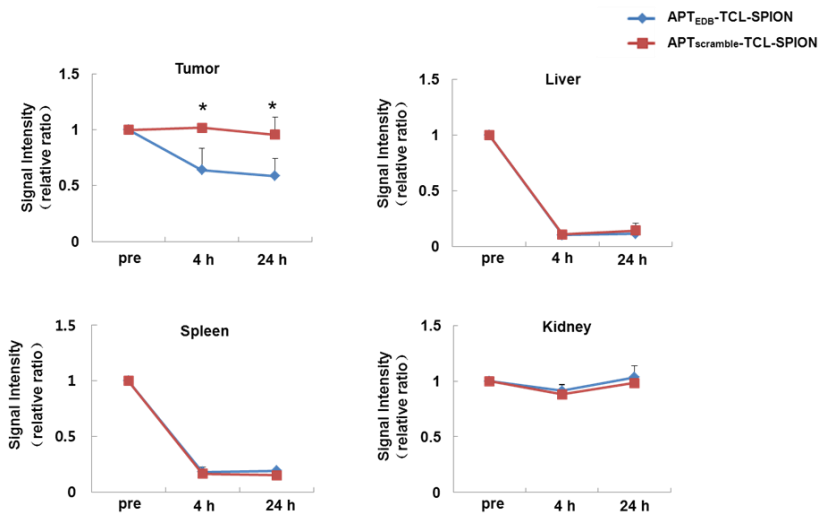

Figure 10: The signal intensity changes of the tumor areas on T_2*-weighted images. An apparent decrease in the signal intensity was detected in APT_{EDB}-TCL-SPION-tumors. All values are presented as the mean ± standard deviation of at least three independent experiments. Asterisks (*) point out that *P* value was statistically significant (<0.05).

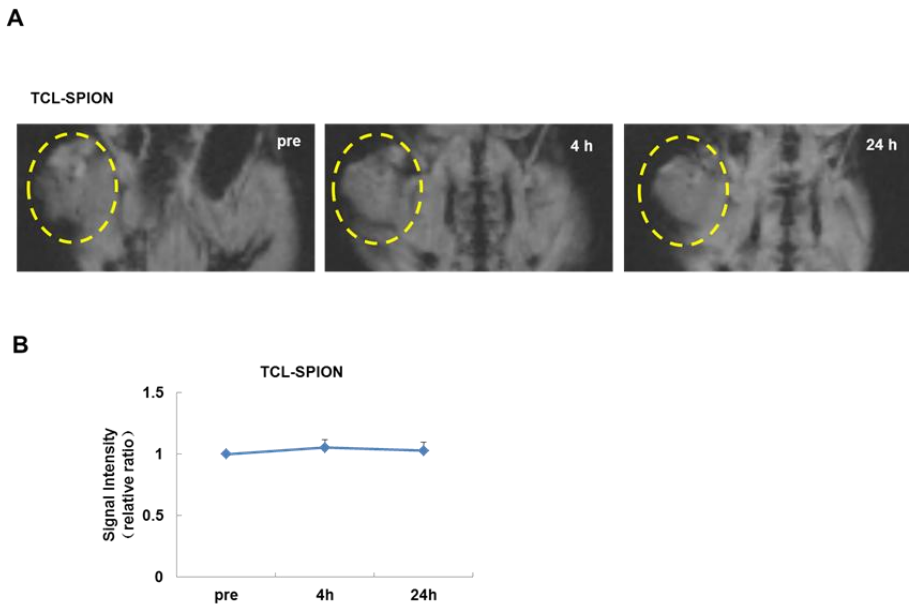

Figure 11: MRI analysis of tumor after injection of TCL-SPION. A: Serial follow-up T_2*-weighted MR images of tumors. B: The signal intensity changes of the tumor areas on T_2*-weighted images. Only marginal changes in the dark signal and signal intensity within the tumor were observed after TCL-SPION injection.

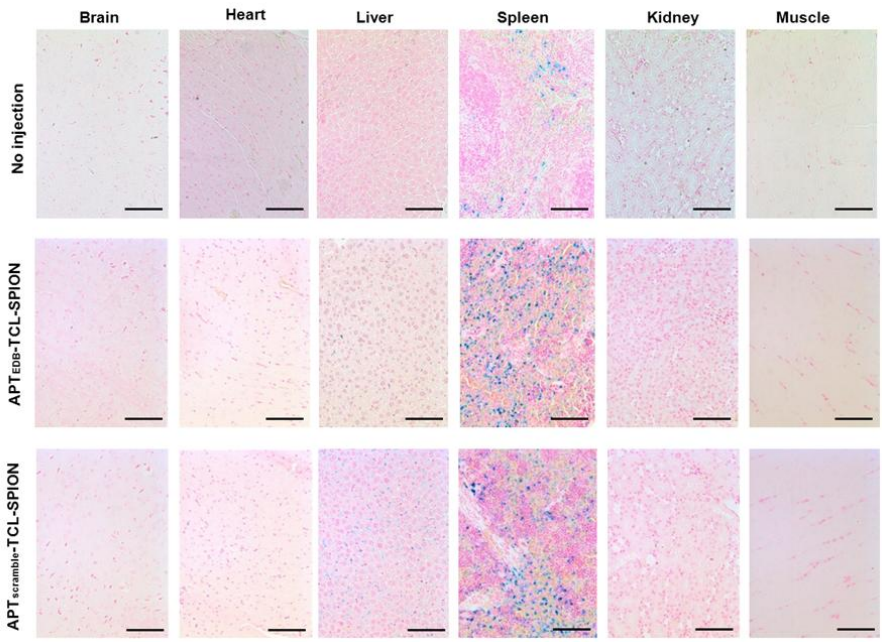

Figure 12: *In vivo* biodistribution of APT_{EDB}-TCL-SPION and $APT_{scramble}$-TCL-SPION. Representative Prussian blue staining of several tissues. Brain, heart, liver, spleen, kidney and thigh muscle were isolated from mouse at 24 h post-injection with APT_{EDB}-TCL-SPION or $APT_{scramble}$-TCL-SPION (20 mg Fe/kg). Accumulated irons were detected as blue dot in microsection of liver and spleen. Scale bar: 100 μm

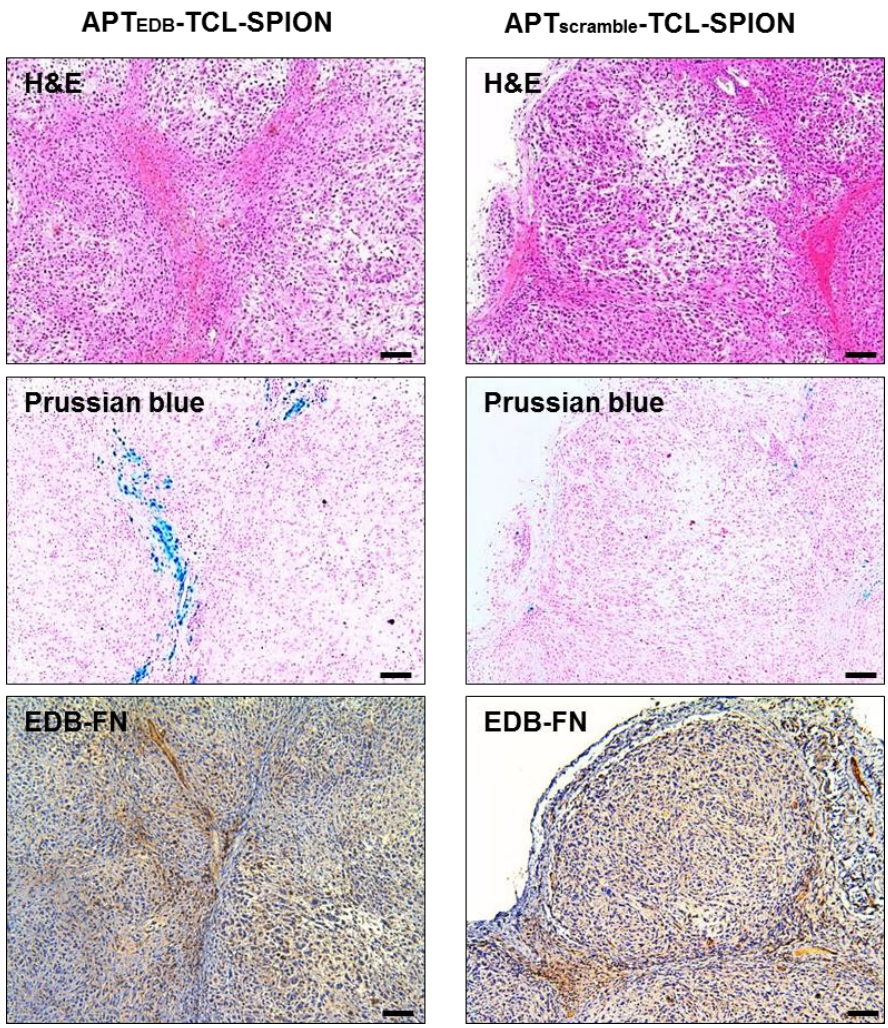

Figure 13: Histological analysis of the tumors. Hematoxylin and eosin (H&E) staining, Prussian blue staining and EDB-FN immunostaining. Tumors were removed at 24 h post-injection with APT_{EDB}-TCL-SPION or $APT_{scramble}$-TCL-SPION (20 mg Fe/kg) after MRI study and histological analysis of the microsectioned

tumor was performed. Prussian blue staining showed that a large number of accumulated nanoparticles were detected as blue dots in the tumors of mice injected with APT_{EDB}-TCL-SPION compared with $APT_{scramble}$-TCL-SPION. Immunostaining of EDB-FN in NDY-1 tumor microsections was performed by using the BC-1 antibody. EDB-FN proteins (dark yellow) were abundantly detected in the NDY-1 tumors injected with APT_{EDB}-TCL-SPION or $APT_{scramble}$-TCL-SPION.

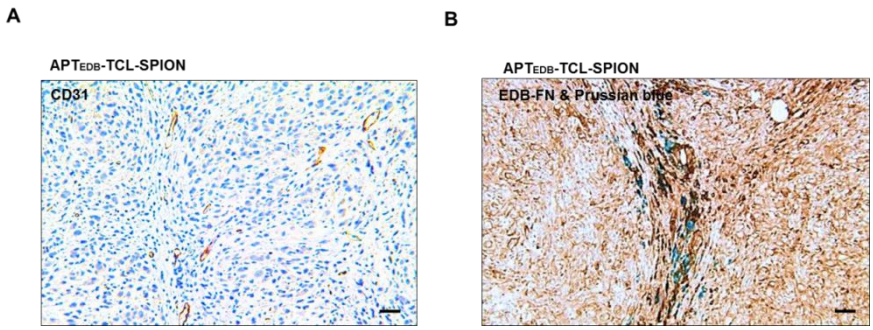

Figure 14: Immunostaining of CD31 and EDB-FN and Prussian blue .

A: Immunostaining of the platelet endothelial cell adhesion molecule (CD31) showed that vessels (dark yellow) were observed in NDY-1 tumors of mice injected with APT_{EDB}-TCL-SPION. B: Co-staining with anti-EDB-FN antibody and Prussian blue. Accumulation of APT_{EDB}-TCL-SPION (blue dots) was observed in EDB-FN positive areas of the tumor vasculature and interstitium. Scale bar: 100 μm

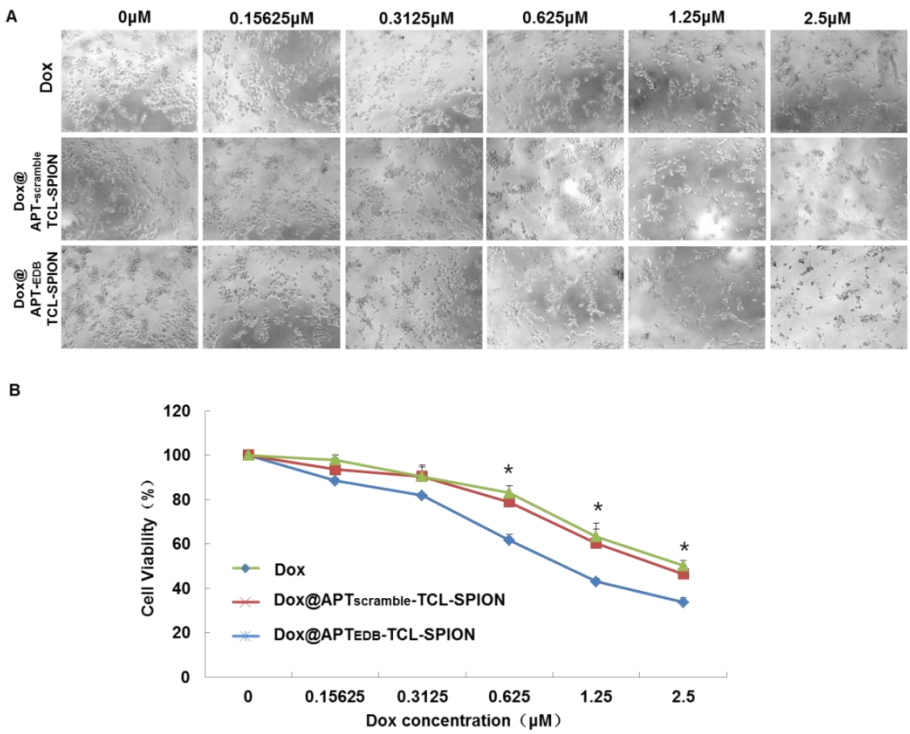

Figure 15: Improved cytotoxicity of Dox@APT$_{EDB}$-TCL-SPION determined by MTT assays. NDY-1cells were incubated with Dox@APT$_{EDB}$-TCL-SPION, Dox@APT$_{scramble}$-TCL-SPIONs or free Dox for 2 h, and then incubated for an additional 24 h. Dox@APT$_{EDB}$-TCL-SPION displayed the improved cytotoxicity in NDY-1 cells as compared to Dox@APT$_{scramble}$-TCL-SPIONs and free Dox. Asterisks (*) point out that *P* value was statistically significant (<0.05)

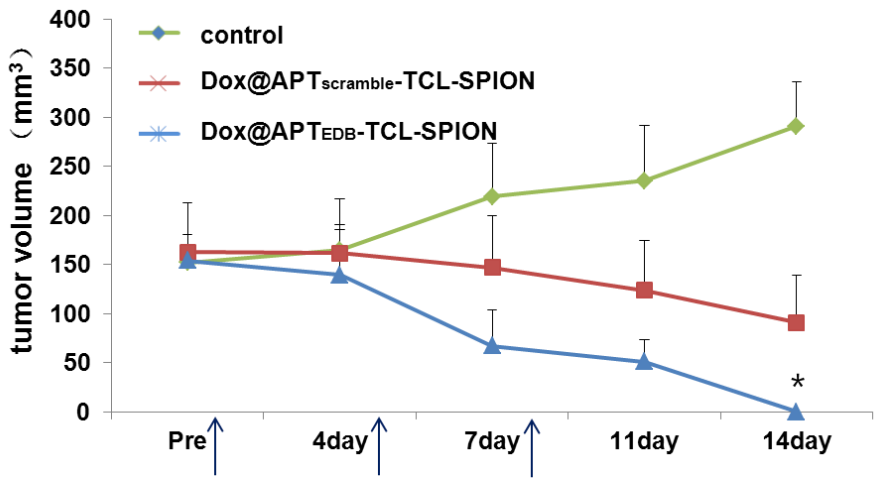

Figure 16: Enhanced antitumor activity of Dox@APT$_{EDB}$-TCL-SPION in the NDY-1 xenograft animal model. When the tumor volumes were about 150 mm^3 at 2 weeks after implantation, tumor volumes were monitored after three intravenous injections with 2 mg Dox/kg Dox@APT$_{EDB}$-TCL-SPION, Dox@APT$_{scramble}$-TCL-SPIONs and 5% glucose at 3-day intervals. An enhanced antitumor effect was detected in Dox@APT$_{EDB}$-TCL-SPION-treated groups. All values are presented as the mean ± standard deviation of at least three independent experiments. Asterisks (*) point out that *P* value was statistically significant (<0.05).

REFERENCES

[1] Al-Hajj M, Wicha MS, Benito-Hernandez A, Morrison SJ, Clarke MF. Prospective identification of tumorigenic breast cancer cells. Proc Natl Acad Sci U S A 2003;100:3983-8.

[2] Dean M, Fojo T, Bates S. Tumour stem cells and drug resistance. Nature reviews Cancer 2005;5:275-84.

[3] Liu H, Patel MR, Prescher JA, Patsialou A, Qian D, Lin J, et al. Cancer stem cells from human breast tumors are involved in spontaneous metastases in orthotopic mouse models. Proceedings of the National Academy of Sciences of the United States of America 2010;107:18115-20.

[4] Ginestier C, Hur MH, Charafe-Jauffret E, Monville F, Dutcher J, Brown M, et al. ALDH1 is a marker of normal and malignant human mammary stem cells and a predictor of poor clinical outcome. Cell Stem Cell 2007;1:555-67.

[5] Potts JR, Campbell ID. Fibronectin structure and assembly. Curr Opin Cell Biol 1994;6:648-55.

[6] Birchler MT, Milisavlijevic D, Pfaltz M, Neri D, Odermatt B, Schmid S, et al. Expression of the extra domain B of fibronectin, a

marker of angiogenesis, in head and neck tumors. Laryngoscope 2003;113:1231-7.

[7] Santimaria M, Moscatelli G, Viale GL, Giovannoni L, Neri G, Viti F, et al. Immunoscintigraphic detection of the ED-B domain of fibronectin, a marker of angiogenesis, in patients with cancer. Clin Cancer Res 2003;9:571-9.

[8] Mhawech P, Dulguerov P, Assaly M, Ares C, Allal AS. EB-D fibronectin expression in squamous cell carcinoma of the head and neck. Oral Oncol 2005;41:82-8.

[9] Kosmehl H, Berndt A, Strassburger S, Borsi L, Rousselle P, Mandel U, et al. Distribution of laminin and fibronectin isoforms in oral mucosa and oral squamous cell carcinoma. Br J Cancer 1999;81:1071-9.

[10] Ricci E, Cavalot AL, Sanvito F, Bussi M, Albera R, Staffieri A, et al. Differential expression and topography of adhesion molecules in laryngeal and oropharyngeal carcinomas. Acta Otolaryngol 2002;122:234-40.

[11] Koukoulis GK, Howeedy AA, Korhonen M, Virtanen I, Gould VE. Distribution of tenascin, cellular fibronectins and integrins in the normal, hyperplastic and neoplastic breast. J Submicrosc Cytol Pathol 1993;25:285-95.

[12] Berndt A, Borsi L, Luo X, Zardi L, Katenkamp D, Kosmehl H. Evidence of ED-B+ fibronectin synthesis in human tissues by non-radioactive RNA in situ hybridization. Investigations on carcinoma (oral squamous cell and breast carcinoma), chronic inflammation (rheumatoid synovitis) and fibromatosis (Morbus Dupuytren). Histochem Cell Biol 1998;109:249-55.

[13] Thakor AS, Gambhir SS. Nanooncology: The future of cancer diagnosis and therapy. CA: a cancer journal for clinicians 2013; [Epub ahead of print].

[14] Yu MK, Park J, Jon S. Targeting strategies for multifunctional nanoparticles in cancer imaging and therapy. Theranostics 2012;2:3-44.

[15] Lee H, Yu MK, Park S, Moon S, Min JJ, Jeong YY, et al. Thermally cross-linked superparamagnetic iron oxide nanoparticles: synthesis and application as a dual imaging probe for cancer in vivo. J Am Chem Soc 2007;129:12739-45.

[16] Li M, Kim HS, Tian L, Yu MK, Jon S, Moon WK. Comparison of Two Ultrasmall Superparamagnetic Iron Oxides on Cytotoxicity and MR Imaging of Tumors. Theranostics 2012;2:76-85.

[17] Wang AZ, Bagalkot V, Vasilliou CC, Gu F, Alexis F, Zhang L, et al. Superparamagnetic iron oxide nanoparticle-aptamer

bioconjugates for combined prostate cancer imaging and therapy. ChemMedChem 2008;3:1311-5.

[18] Yu MK, Kim D, Lee IH, So JS, Jeong YY, Jon S. Image-guided prostate cancer therapy using aptamer-functionalized thermally cross-linked superparamagnetic iron oxide nanoparticles. Small 2011;7:2241-9.

[19] Yu MK, Park J, Jeong YY, Moon WK, Jon S. Integrin-targeting thermally cross-linked superparamagnetic iron oxide nanoparticles for combined cancer imaging and drug delivery. Nanotechnology 2010;21:415102.

[20] Kim S, Kim D, Jung HH, Lee IH, Kim JI, Suh JY, et al. Bio-inspired design and potential biomedical applications of a novel class of high-affinity peptides. Angew Chem Int Ed Engl 2012;51:1890-4.

[21] Park J, Kim S, Saw PE, Lee IH, Yu MK, Kim M, et al. Fibronectin extra domain B-specific aptide conjugated nanoparticles for targeted cancer imaging. Journal of controlled release : official journal of the Controlled Release Society 2012;163:111-8.

[22] Saw PE, Kim S, Lee IH, Park J, Yu M, Lee J, et al. Aptide-conjugated liposome targeting tumor-associated fibronectin for glioma therapy. J Mater Chem B 2013;1:4723-6.

[23] Neve RM, Chin K, Fridlyand J, et al. A collection of breast cancer cell lines for the study of functionally distinct cancer subtypes. Cancer Cell. 2006;10:515-27.

[24] Lee KM, Han W, Kim JB, Shin I, Ko E, Park IA, et al. The CD49d+/high subpopulation from isolated human breast sarcoma spheres possesses tumor-initiating ability. International journal of oncology 2012;40:665-72.

[25] Choi Y, Kim HS, Cho KW, Lee KM, Yi YJ, Eun SJ, et al. Noninvasive identification of viable cell populations in docetaxel-treated breast tumors using ferritin-based magnetic resonance imaging. PLoS One 2013;8:e52931.

[26] Hauger O, Delalande C, Deminiere C, et al. Nephrotoxic nephritis and obstructive nephropathy: evaluation with MR imaging enhanced with ultrasmall superparamagnetic iron oxide-preliminary findings in a rat model. Radiology. 2000;217:819-26

[27] Weissleder R, Stark DD, Engelstad BL, et al. Superparamagnetic iron oxide: pharmacokinetics and toxicity. AJR Am J Roentgenol. 1989;152:167-73.

[28] Eccles SA, Aboagye EO, Ali S, et al. Critical research gaps

and translational priorities for the successful prevention and treatment of breast cancer. Breast Cancer Res. 2013;15:R92.

[29] Neri D, Carnemolla B, Nissim A, et al. Targeting by affinity-matured recombinant antibody fragments of an angiogenesis associated fibronectin isoform. Nat Biotechnol. 1997;15:1271-5.

[30] Birchler M, Neri G, Tarli L, et al. Infrared photodetection for the *in vivo* localization of phage-derived antibodies directed against angiogenic markers. J Immunol Methods. 1999;231:239-48.

[31] Chames P, Van Regenmortel M, Weiss E, et al. Therapeutic antibodies: successes, limitations and hopes for the future. Br J Pharm. 2009;157:220-33.

[32] McCarthy JR, Bhaumik J, Karver MR, et al. Targeted nanoagents for the detection of cancers. Mol Oncol. 2010;4:511-28.

[33] Benachour H, Seve A, Bastogne T, et al. Multifunctional Peptide-conjugated hybrid silica nanoparticles for photodynamic therapy and MRI. Theranostics. 2012;2:889-904.

[34] Zheng Y, Liu Y, Jin H, et al. Scavenger receptor B1 is a potential biomarker of human nasopharyngeal carcinoma and its growth is inhibited by HDL-mimetic nanoparticles. Theranostics. 2013;3:477-86.

[35] Goscin CP, Berman CG, Clark RA. Magnetic resonance imaging of the breast. Cancer Control. 2001;8:399-406.

[36] Goodarzi N, Ghahremani MH, Amini M, Atyabi F, Ostad SN,

Shabani Ravari N, et al. CD44-Targeted Docetaxel Conjugate for Cancer Cells and Cancer Stem-Like Cells: A Novel Hyaluronic Acid-Based Drug Delivery System. Chem Biol Drug Des. 2014; [Epub ahead of print].

[37] McLaughlin R, Hylton N. MRI in breast cancer therapy monitoring. NMR Biomed. 2011;24:712-20.

국문초록

서론: 유방암줄기세포를 식별하는것은 유방암진단과 치료에 있어서 중요한 과제다. 본 연구에서는 유방암줄기세포를 동정할수 있는 새로운 바아오마커(biomarker)인 피브로넥틴의 엑스트라 도메인 B (fibronectin extra domain B, EDB-FN)를 선택적으로 표적하는 앱타이드(APT_{EDB})를 결합하고 항암제(doxorubicine; Dox)를 선적한 다기능성 산화철나노입자(TCL-SPION)를 이용하여 체외(in vitro)와 생체내(in vivo)에서 자기공명영상으로 유방암줄기세포를 진단할수 있으며 동시에 치료할수 있는지를 규명하고자 한다.

실험방법 및 결과: 사람유래 유방암줄기세포(NDY-1) 및 유방암 세포주(MCF-7, BT-474, SUM-225, MDA-MB-231)에서 RT-PCR 과 ALDEFLUOR assay 방법을 이용하여 자가생존관련 유전자, 유방암줄기세포 특이유전자 및 EDB-FN 의 발현을 분석한 결과 NDY-1 세포는 자가생존능력(Nanog, Oct4, KLF4) 및 유방암줄기세포 표현형(CD24-/CD44+)과 ALDH1 활성을 나타냈으며 특히 다른 유방암세포와 달리 EDB-FN 이 많이 발현되였다. EDB-FN 을 선택적이고 특이적으로 표적하는 앱타이드(APT_{EDB})에 적색 형광물질(Cy3.3)로 표지하여 실험한 결과 NDY-1 세포만 선택적으로 타겟되는것을 형광이미지로 확인하였다. 또한 세포 팬텀을 제작하고 임상용 3T MR 장비로 T_2 강조영상을 획득하고 T_2 값을 분석한 결과

APT_{EDB-}TCL-SPION 를 처리한 NDY-1 에서는 현저한 조영증강 효과를 관찰하였으나 EDB-FN 을 발현하지 않는 MCF-7 에서는 조영증강 효과를 관찰할수 없었다. 유방암줄기세포를 자기공명영상으로 진단할수 있는지를 평가하기 위해서 NDY-1 세포를 면역결핍마우스(BALB/c nude)의 피하에 이식하여 종양을 유발한 다음 20 mg Fe/kg 농도의 APT_{EDB-}TCL-SPION 과 $APT_{scramble-}$TCL-SPION 를 각각 마우스의 꼬리정맥으로 투여하고 임상용 3T MR 장비로 T_2^*강조영상을 획득하고 Signal Intensity 를 분석한 결과 APT_{EDB-}TCL-SPION 을 투여한 마우스의 종양에서 현저한 조영증강 효과를 관찰할수 있었으나 $APT_{scramble-}$TCL-SPION 을 투여한 종양에서는 조영증강 효과가 관찰되지 않았다. 마지막으로 진단과 동시에 유방암줄기세포 치료효과를 평가하기 위해서 EDB-FN 을 표적하는 APT_{EDB} 와 항암제(Doxorubicin; Dox)를 선적한 Dox@APT_{EDB}-TCL-SPION 를 생산하여 체외(in vitro)와 생체내(in vivo)에서 치료효과를 분석한 결과 DOX@$APT_{scramble-}$TCL-SPION 와 비교하여 Dox@APT_{EDB}-TCL-SPION 에서 세포생존율이 많이 감소한것을 확인하였으며 종양 동물모델에서도 종양의 성장이 억제되고 종양크기가 감소하는 성공적인 종양 치료효과를 확인하였다 .

결론: 본 연구결과를 통해 EDB-FN 는 유방암줄기세포의 새로운 biomarker 로 제시되며 EDB-FN 을 선택적으로 표적할수 있는 APT_{EDB} 를 접합시키고 항암제를 선적한 다기능성산화철 나노입자 Dox@APT_{EDB-}TCL-SPION 를 사용하여 EDB-FN 을 발현하는

유방암줄기세포를 MRI 로 진단할수 있으며 동시에 치료효능까지 평가할수 있었다. 앞으로 유방암줄기세포를 표적할수 있는 리간드를 결합시킨 나노입자에 항암제뿐만 아니라 유전자 치료제를 선적함으로써 유방암줄기세포를 동정하고 표적치료효과를 증대시킬수 있을것으로 기대된다.

주요어: 앱타이드, 유방암줄기세포, 피브로넥틴의 엑스트라 도메인 비, 초상자성나노입자, 자기공명영상, 독소루비신

학번: 2013-30810